Article

Fluorescent Probe for Transmembrane Dynamics During Osmotic Effects

Eva Palacios-Serrato, Daniela Araiza Olivera, and Arturo Jiménez-Sánchez

Anal. Chem., **Just Accepted Manuscript** • DOI: 10.1021/acs.analchem.9b05390 • Publication Date (Web): 30 Jan 2020

Fluorescent Probe for Transmembrane Dynamics During Osmotic Effects

Eva Palacios-Serrato, Daniela Araiza-Olivera and Arturo Jiménez-Sánchez*

Instituto de Química - Universidad Nacional Autónoma de México.
Circuito Exterior s/n, Coyoacán 04510. Ciudad Universitaria, Ciudad de México, México. E-mail: arturo.jimenez@iquimica.unam.mx

ABSTRACT: Membrane tension pores determine the organelles dynamics and function giving rise to physical observables during cell death process. While fluorescent organelle-targeted probes for specific chemical analytes are increasingly available, subcellular dynamic processes involving not only chemical but physicochemical and physical parameters are uncommon. Here we report a mitochondrial chemical probe, named **RCN**, rationally designed to monitor the osmotic effects during the transmembrane tension pore formation by using local mitochondrial polarity and a subcellular localization redistribution property of the probe. Utilizing fluorescence spectroscopy, high-resolution confocal imaging and spectrally-resolved confocal microscopy we provide a new correlation between mitochondrial dynamics and bleb vesicles formation with osmotic pressure stimuli in the cell, where the mitochondrial local polarity resulted to be drastically increased. The **RCN** provides a reliable protocol to assess the transmembrane pore formation driven osmotic pressure increments though local polarity variations, a more robust physicochemical parameter allowing to measure the health and decease status of the cell.

Cells and subcellular structures are delimited by lipid bilayers which determine organelle dynamics such as motility, fusion/fission of the organelle framework, morphology and volume, and inter-organelle contacts.[1-7] Membrane tensional status as well as tension pores are then major regulators of the organelle dynamics.[8,9] Although the mechanical forces governing subcellular interactions is an emerging area,[8-11] now the fact that membrane tension regulates membranous organelles' function, is well established. Examples reporting the organelle tensional status have been reported.[8-13] However, the way tensional status of an organelle membrane modifies subcellular function and dynamics is still an unmeet need. In fact, the appearance of transmembrane tension pores is determined by the influx of water molecules into the cell, giving rise to an augmented membrane tension and local polarity (in terms of dielectric constant).[14-16] The organelle shape variations and different osmotic phenomena such as the formation of transient tension pores and vesicle rupture[17] comprise a common physical observation during cell death process.[18] Monitoring such tension stimuli-responsive scenario is challenging since the transmembrane tension pores, with their effective radii that are comparable to the size of small molecules and ions, have size selective properties[19-21] which increase the plasma membrane permeability, specially for ions and small molecules, thus disbalancing the electrochemical gradients of the cell. For this reason, the functional visualization and monitoring of transmembrane dynamics upon tensional stimuli using common fluorescent organelle localizers is tremendously difficult as they exhibit signal interferences and artefacts due to the local membrane potential depolarization during tension stimuli. Deservingly so, the correlation of transmembrane tension pores with dynamic properties such as local polarity helps to understand the tensional status in terms of membrane function.[8] The local polarity monitoring serves as a general reporter of all the osmotically driven ions and molecules for which any membrane is selective. Then, local polarity is a more useful bioanalitycal parameter of osmotically perturbed membrane function during a specific cell stage, *i.e.* cell proliferation or cell death process. More importantly, mitochondrial dynamics is directly affected during the osmotic variations inside the cell where both, the tensional and local polarity status of the organelle is substantially altered. In fact, the inflow of K^+ ion increases the mitochondrial osmotic pressure, which results in the formation of the so-called donut-shaped mitochondria.[22,23] Also, the osmotic energy gained from K^+ ion inflow leads to an increase of mitochondrial volume. Then, fast-response fluorescent probes able to monitor mitochondrial dynamics and function during tensional and osmotic stimuli could be helpful to understand cell death process, cell bleb formation and how mechanical forces regulate cell membrane status.

Herein, we describe a mitochondrial fluorescent probe, called **RCN** (Scheme 1), that follows a sensing mechanism aimed to monitor the osmotic effects on the transmembrane tension pore formation by using local mitochondrial polarity and a subcellular localization redistribution property of the probe. The **RCN** consists of a chromenylium-cyanine structure derived from a cinnamic-chromenylium-cyanine (*RCin* fragment) and a naphthalimide (*Naph* fragment), Figure 1. By itself, the *RCin* exhibits highly tunable optical properties, *i.e.* high solvatochromic effects, large Stoke shifts, a well-defined dual-fluorescent behavior which can be promoted either by Kasha rule breaking, intramolecular proton transfer or intramolecular charge transfer.[24] However, the chromenylium-cyanine structure usually results in very low fluorescent quantum yields (Φ_f of *RCin* = 0.01). On the other side, the *Naph* fragment exhibits a high Φ_f of 0.63 (Supplementary Information file) avoiding a versatile photophysical scheme, thus acting as a fluorescent signal enhancer. The solvatochromic, polarity-dependent *RCin* fragment shows mitochondria specific localization in the red confocal channel as a consequence of its chromenylium ion identity while the *Naph* fragment equilibrates the cytosol and nucleoli in the green confocal channel. When tether these fluorophores into **RCN**, the whole construct shows a clean mitochondrial localization under green and red confocal channels with bright emission (Φ_f of 0.45) and excellent photostability (see Figure S1, SI). The mitochondrial co-localization analysis using MitoLite™ Blue stain as well as functional mitochondrial co-localization dynamic using mitochondrial membrane potential uncoupling stimulus are shown in Figure S2.

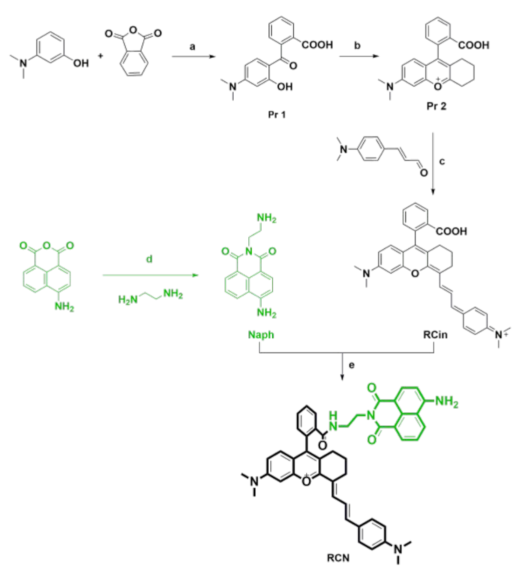

Scheme 1. Structures and synthetic methodology to obtain **RCN** probe: (a) Toluene, 120 °C, 24 h; then NaOH (30% aq), 90 °C, 12 h; (b) H_2SO_4, 60 °C, 2.5h, then $HClO_4$; (c) acetic anhydride, 60 °C, 3 h; (d) 120 °C, 6h; (e) Cs_2CO_3, HBTU, DMF, 90 °C, 24 h.

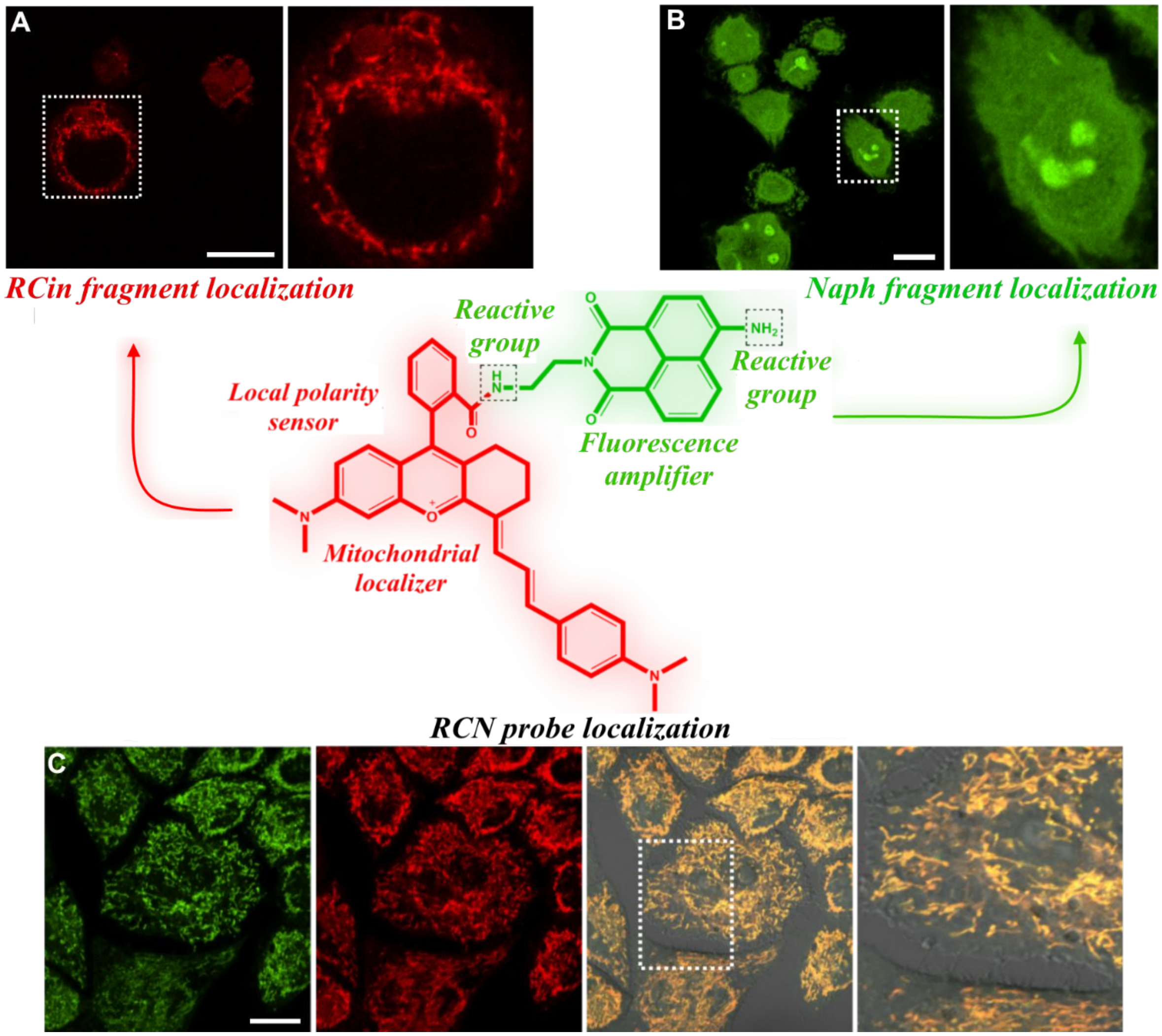

Figure 1. Chemical structure of the **RCN** probe and its localization. (A) The solvatochromic, polarity-dependent *RCin* fragment shows a mitochondria specific localization in the red confocal channel. (B) With high fluorescence quantum yield, the *Naph* fragment equilibrates the cytosol and nucleoli in the green confocal channel. (C) The whole construct **RCN** exhibiting mitochondrial localization under green and red confocal detection. Mitochondrial co-localization analysis is shown in Figure S2, SI file. Scale bars represent 20 µm.

EXPERIMETAL SECTION

Materials and Methods. All starting reagents were obtained from commercial suppliers and used as received.

Synthesis. The **RCN** probe was synthesized according to Scheme 1. Detailed description and chemical characterization are presented in the Supplementary Information file.

Optical spectroscopy. Absorption spectra were acquired in a 10 mm path-length quartz-cell Cary-50 (Varian) spectrophotometer, the emission and excitation spectra were obtained in an Edinburgh Instruments FS500 fluorimeter at room temperature (20 ± 1 °C) under aerated conditions.

Cell Culture and Confocal Microscopy. HeLa cells as well as live human pulmonary adenocarcinoma epithelial cells (SK-LU-1) were cultured in RPMI-1640 medium (RPMI Medium 1640 (1x), Gibco, Gaithersburg MD) supplemented with 10% fetal bovine serum (FBS, Invitrogen, Carlsbad CA), L- glutamine (2 μM), penicillin G (100 u/mL), streptomycin sulfate (100 μg/ mL) at 37°C with 5% v/v CO_2. Live SK-LU-1 cells were seeded on 8 Petri dishes of 5 cm diameter with glass bottom for 36 hours before experiments using RPMI-1640 medium supplemented. Then, specific concentrations of **RCN** from 5 to 8 μM were used. Commercial specific organelle localizers were added on each Petri dish 45 minutes before imaging experiments. All dishes were washed two times with RPMI. During confocal imaging, microscope parameters were maintained constant and excitation light was fully-shielded to prevent laser artefacts. Live HeLa cells were seeded in 8 well μ–slides (iBidi, Germany) at a density of 20000 cells per well one day prior to experiments in MEM alpha with 10% FBS. On treatment day, cells were washed once in MEM alpha with no FBS and incubated with 5 to 8 μM probe **RCN** for 30 minutes. For experiments with MitoLite® Blue (Thermo Fisher Scientific), 10 nM were added 10 minutes before **RCN**. Cells were then washed twice in MEM alpha with no FBS and imaged maintaining 5% CO_2 and 37°C during the experiments using an inverted Zeiss LSM 880 microscope or a Nikon A1R upgraded with a spectral detector unit. On treatment day for fluorescence time course experiments, cells were incubated with 7 μM probe **RCN** for 30 minutes in MEM alpha with 5% FBS for the indicated time at 37°C with 5% CO_2, then imaged at the same conditions.

RESULTS AND DISCUSSION

Spectroscopic features of the RCN probe. As mentioned, the *RCin* contribution to **RCN** emission profile allows a strong solvatochromic effect, *i.e.* the emission maximum (λ_{em}) of the *RCin* in hexane is 400 nm while in methanol is 795 nm, a difference of *ca.* 12,500 cm^{-1} (400 nm) with intermediate emission maximum wavelengths for other solvents, Figure 2A and S3. However, such extremely high and unusual solvatochromic effect turns out to be diminished to some extent in **RCN** since the main emission feature is the fluorescence intensity coming from the *Naph* fragment although the solvatochromic effect is still high for the whole **RCN** construct. In fact, a significant sensitivity to solvent polarity was observed, Figure 2B-C. In order to calibrate such fluorescence response under variable polarity, we performed the calibration of polarity effect using organic solvents with different dielectric constant for **RCN** and *RCin* fragment, Figure 2B-C. Also, dioxane : water system calibration gave similar calibration curves, Figure S4, SI file. The **RCN** probe exhibits a dual-band fluorescence profile with a strong enhancement in the visible region as the polarity of the solvent decreased while the NIR emission was quenched, Figure 2B. The ratio of fluorescence intensity at 515 nm versus 715 nm upon variable dielectric constant was then quantified observing a linear relationship with a regression coefficient of $R^2 = 0.987$. Importantly, the 200 nm difference of fluorescence wavelength recordings for the calibration plot is large enough to be suitable for confocal ratiometric imaging correlations of subcellular environments with no confocal channel interference. A similar result was observed for the isolated *RCin* fragment, here the fluorescence ratio at 750 nm versus 500 nm reproduce a similar dielectric constant dependence with a linear relationship of $R^2 = 0.995$. In fact, using ratiometric confocal imaging, both isolated fluorophores (**RCN** and *RCin*) can be used as local polarity reporters on mitochondria where comparison of those polarity calibrations can afford a more robust measurement. Then, mitochondrial local polarity was monitored with the fluorescent profile of **RCN** under conditions promoting osmotic pressure variations through transmembrane pore formation in order to evaluate the probe to track dynamic changes that eventually cause strong morphological changes and pronounced physicochemical variations in the organelle microenvironment.[25,26]

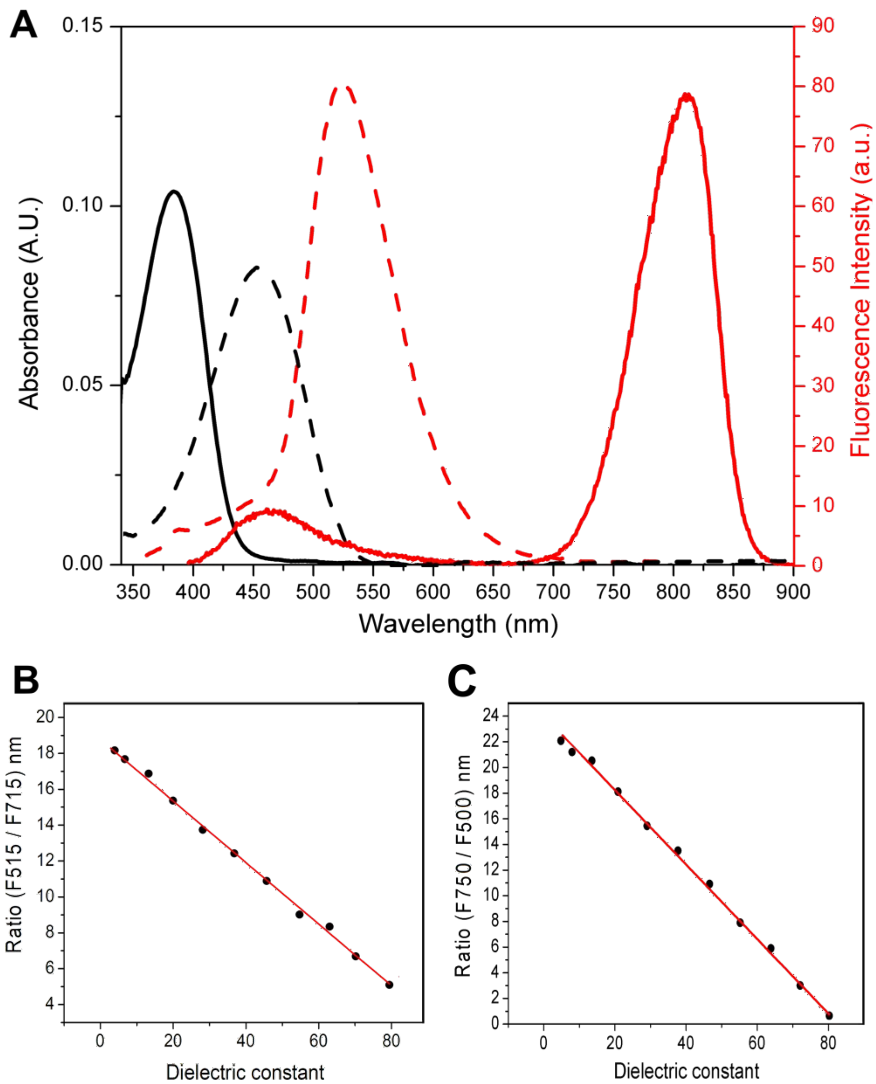

Figure 2. UV-Vis (black lines) and fluorescence (red lines, λ_{ex} = 380 nm) spectra in methanol for the *RCin* (solid lines) and the *Naph* (dashed lines) fluorophore units (A). Calibration of the polarity effect using organic solvents with different dielectric constant for **RCN** (B) and *RCin* (C). Water : dioxane calibration as a function of dielectric constants is presented in Figure S4, SI file.

On the other hand, the viscosity effect on the **RCN** probe was also assessed by the acetone : glycerol continuous variation, which is a solvent mixture having a larger dielectric constant difference compared to methanol : glycerol. Fluorescence spectra are presented in Figure S3-C, where no significant fluorescence increment was observed in both, green and red channels. Then, a Catalán scale analysis was also implemented, which comprises a more quantitative solvent interaction scheme. Solvents of different viscosity and dielectric constant were used, Figure S3-B.

The correlation coefficients for fluorescence maximum observable did not show significant changes when *considering* the viscosity parameter of the solvents compared to the correlation *without considering* the viscosity effect, this indicates that solvent viscosity has no influence on the polarity (Table S1, SI file).

Mitochondrial dynamics and bleb formation upon tension stimuli in epithelial cells. The membrane tension was stimulated by osmotic pressure increments. If the pressure in the cell is being continuously increased at a point disturbing the membrane binding to the cytoskeleton, the membrane detaches from it, then starts stretching and a bleb vesicle is formed.[27,28] While the bleb formation can be initiated by a cell volume increment, the mechanism necessarily involves an osmotic pressure increment by the simultaneous formation of transmembrane pores.[18] Then, to carefully initiate the bleb formation process we used nystatin, a transmembrane pore-forming agent, especially acting on the plasma and mitochondria. However, the mitochondrial dynamics is consequently altered by this process and to the best of our knowledge, no fluorescent probes able to follow bleb formation and mitochondrial dynamics by staining both entities have been reported to date. Our studies on intracellular communication using fluorescent probes indicated that **RCN** probe continuously localized mitochondria during nystatin treatment, thus allowing functional visualization of bleb formation, Figure 3. As can be seen, the donut-shape mitochondrial network is clearly formed after 30 minutes treatment as shown in the green and red confocal channels. However, the **RCN** fluorescence profile indicate two different probe distribution patterns. In the green- and red-channels, the mitochondrial network and bleb membrane were observed, while a clean and structured nuclear distribution was only observed in the green-channel, Figure 3A. This phenomenon suggests the **RCN** probe to be fragmented into the *Naph*- and *RCin*-type entities promoted by the nystatin treatment since the green and red emission signal is the same as the one observed for *RCin*, and the *Naph* green emission is located in the nuclei. In fact, Figure 3A shows a brighter green emission in the nuclei (similar to *Naph* signal) compared to the *RCin* low intensity green-channel emission located in the mitochondrial network.

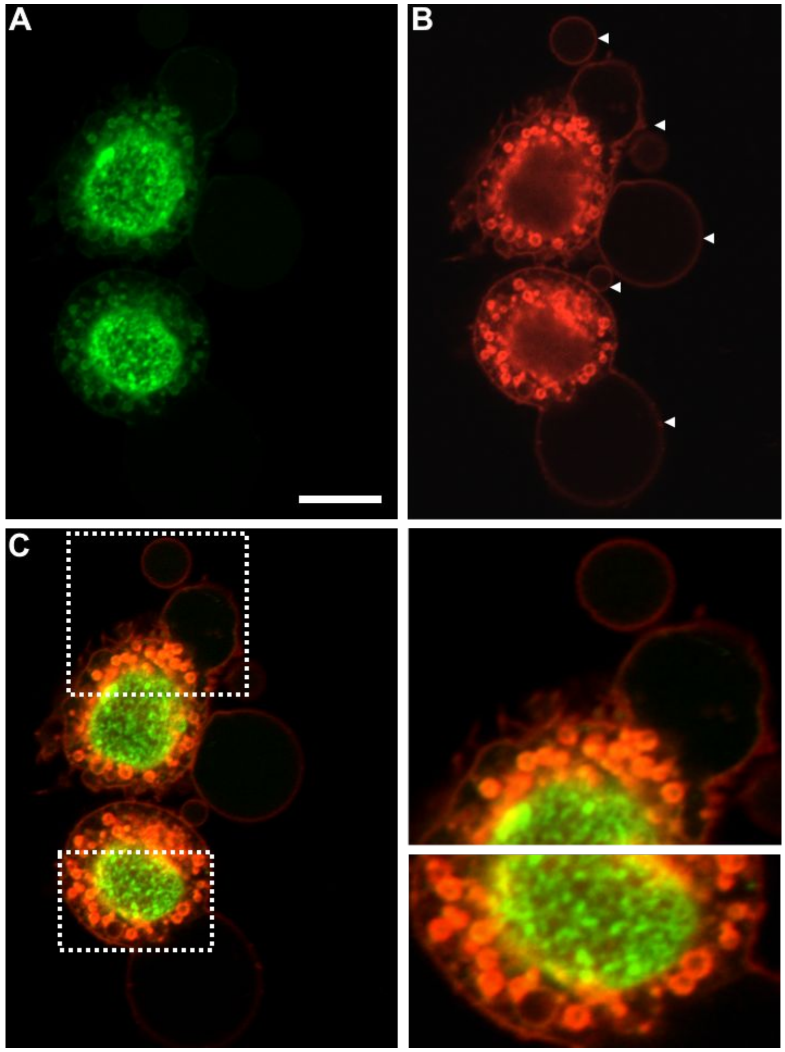

Figure 3. Confocal images of 5 µM **RCN** in SK-Lu-1 cells under 1 hour 100 µM nystatin treatment in the (A) green and (B) red-channels. (C) Merge image with insets showing mitochondrial donut formation with major red emission contribution and green signal redistribution into the nucleus. Mitochondrial co-localization analysis is shown in Figure S2, SI. Scale bars represent 20 µm.

Furthermore, not only the mitochondrial shape and dynamics is altered during transmembrane pore formation, but such osmotic variations induced a homogeneous increment in the cell volume observed in few minutes (5 to 15 minutes time scale) giving rise to the vesicle leakage prior to cell lysis. Figure 4 shows a time-course experiment taken between 0 and 25 minutes after low-dose nystatin addition using high-resolution confocal microscopy. Firstly, the bright field allows to follow the general cell-shape alterations and the green and red-channels evidencing the **RCN** emission profile located in mitochondria.

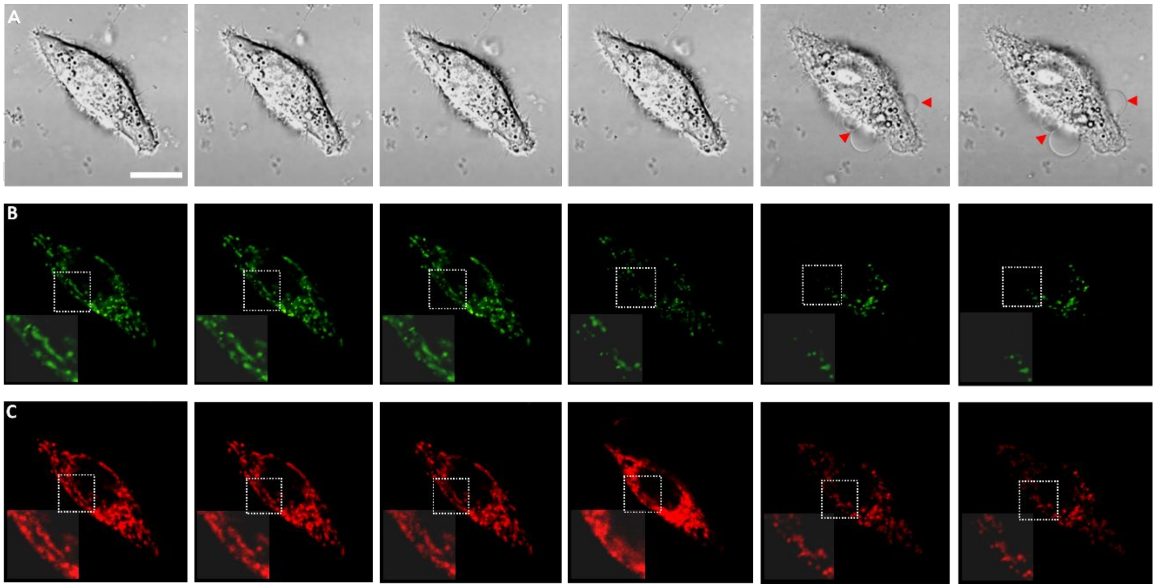

Figure 4. Confocal images of 5 μM **RCN** in SK-Lu-1 cells under 25 minutes low-dose 50 μM nystatin treatment observed in the (A) bright field, (B) green- and (C) red-channels taken at time t_0 = 0 min, then each 5 min until t_5 = 25 min. Insets show the indicated expansion to visualize a mitochondrial fragmentation and motility due to swelling process. Excitation light was fully shielded between recordings to prevent artefacts and photobleaching. Organelle morphology (form factor) analysis is presented in Figure S5. Scale bar represents 20 μm.

Although both, mitochondrial and bleb swelling were observed, the mitochondrial dynamics was altered to a greater extent. A form factor (*F*) analysis indicated a relatively larger *F* value (defined as $P^2/4\pi A$, where P is the perimeter and A is the area of a single mitochondrion) of *ca.* 50% after nystatin treatment. This is because the increment in the osmotic pressure achieved by the inflow of K^+ ions results in both, mitochondrial donut formation and swelling. As the fluorescent staining observed for the membrane blebs required a higher laser potential to be properly observed, we utilized a higher concentration of **RCN** before nystatin treatment in order for the blebs to be well-contrasted under the green channel setup using low laser power conditions, Figure 5. These conditions also allowed a slight nucleoli visualization and the in-plane bleb illumination provided a bright and clean emission on these membranes, while the mitochondrial framework was observed in the red-channel setup, the channels overlap is shown in Figure 5D.

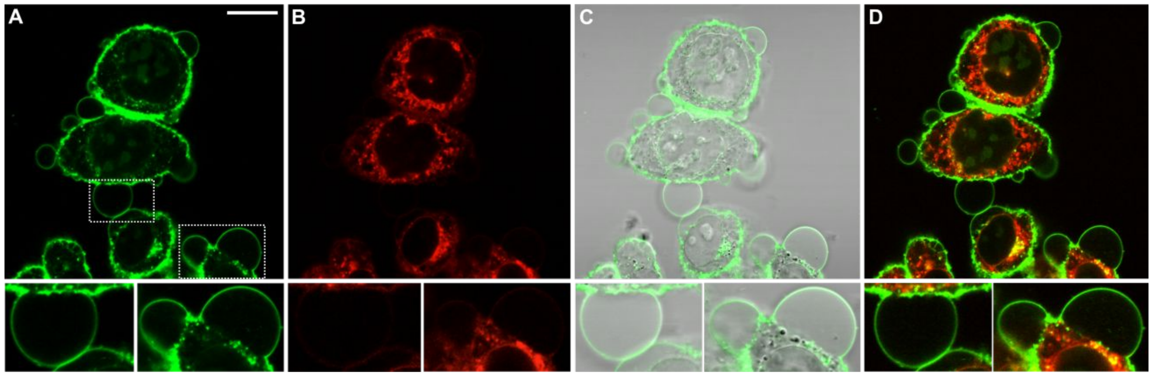

Figure 5. Confocal images of 8 μM **RCN** in SK-Lu-1 cells under 25 min 100 μM nystatin treatment in the (A) green- (B) red- and (C) bright-channels. (D) Green and red merged image showing bleb formation and morphologically altered mitochondrial framework, respectively. Insets show the indicated expansions. Scale bar represents 20 μm.

As this probe fragmentation was observed after treatment of high-dose nystatin up to the cell death process is initiated, we hypothesized that proteases were responsible for such probe rupture.[29] Then, effector proteases can break peptide bonds such as the one present in **RCN**.[30] Structural analysis of **RCN** interaction with protease k by high resolution mass spectrometry and fluorescence spectroscopic revealed the formation of *Naph*, *RCin* and an *RCin*-derived oxonium ion, the fluorescence titration of proteinase k to **RCN** probe also suggested the activation of the isolated *Naph* emission, Figures S6-S8.

Ratiometric confocal imaging experiments were then correlated before and after nystatin treatment, *i.e.* using the **RCN** and *RCin* polarity calibration profiles. Before nystatin treatment, using the **RCN** profile the local polarity (in terms of dielectric constant) was determined to be $\varepsilon = 16.1 \pm 0.6$. To note, a similar result was found when using the *RCin* profile, with a $\varepsilon = 18.8 \pm 0.5$. Such difference could be a consequence of the higher feasibility of the *RCin* to be solvated by polar species in its surrounding, giving a high dependency in the polar region since the dipole moment is located on the longitudinal π-conjugated axis (from the dimethylamino-cinnamic to the dimethylamino-chromenylium moieties) which is in-plane. The **RCN** probe, on the other hand, has this dipole moment in contact with the *Naph* electronic density, thus relocalizing it out of the

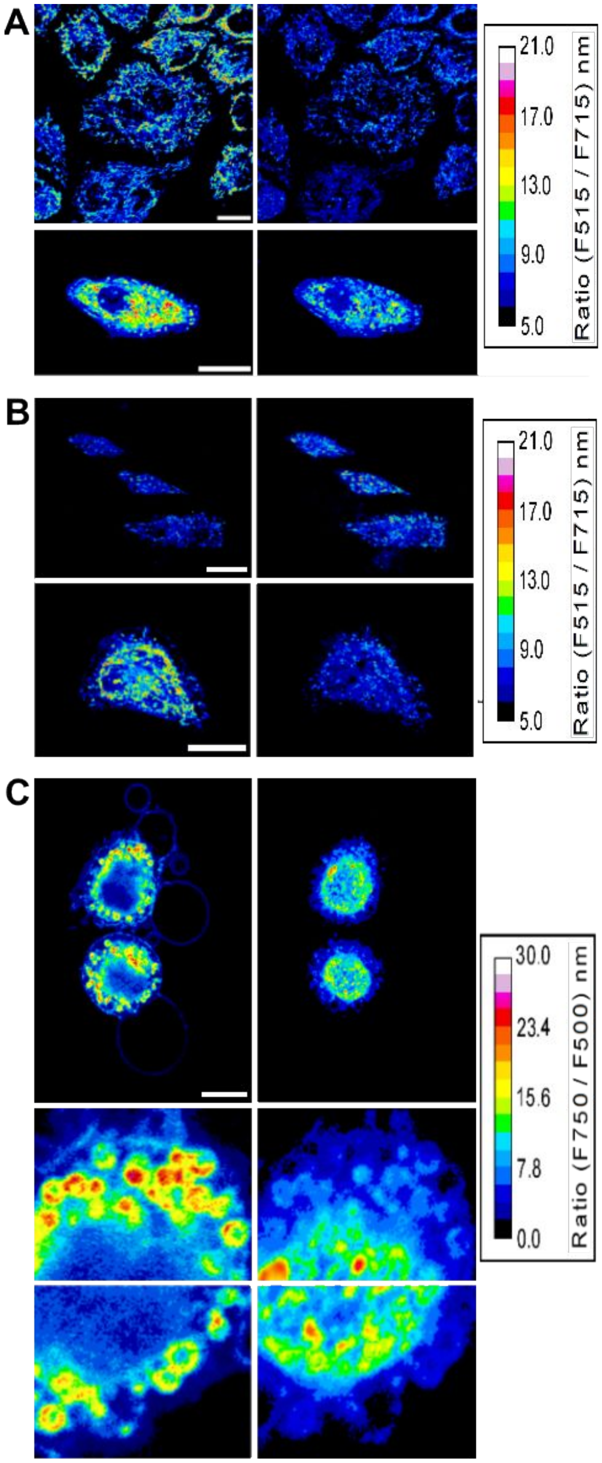

Figure 6. Ratiometric confocal imaging to study the effect of osmotic pressure increments through transmembrane pore formation by nystatin agent on the mitochondrial polarity of live cells stained with 5 μM **RCN**. Pseudo-color images show changes in polarity: (A) HeLa cells before and after 30 min treatment; (B) SK-Lu-1 cells before (left) and after (right) 30 min treatment and (C) SK-Lu-1 during donut-shape formation at 45 min (left) and 60 min (right) treatment. Scale bars are 20 μm.

molecular plane. Significant polarity increments were obtained after nystatin treatment, finding the dielectric constants of 30.7 ± 0.8 and 33.5 ± 0.6 with **RCN** and *RCin* probes, respectively, Figure 6.

To corroborate the ratiometric analysis we implemented spectrally-resolved confocal microscopy experiments since one of the main drawbacks in the confocal ratiometric analysis is the loss of the probe structural information and local spectral-resolution during time-course experiments, particularly when the fluorophore chemically interacts with a given stimuli or is being fragmented. In this sense, spectrally-resolved imaging gives analytical bioimaging the ability to perform *in-situ* calibration, thus allowing continuous structural information of the probe response profiles. Using a confocal array coupled with a spectral detector unit, accurate spectral unmixing enabled **RCN** to be spectrally resolved in real time with 32- channel images of 512x512 pixels, Figure 7.

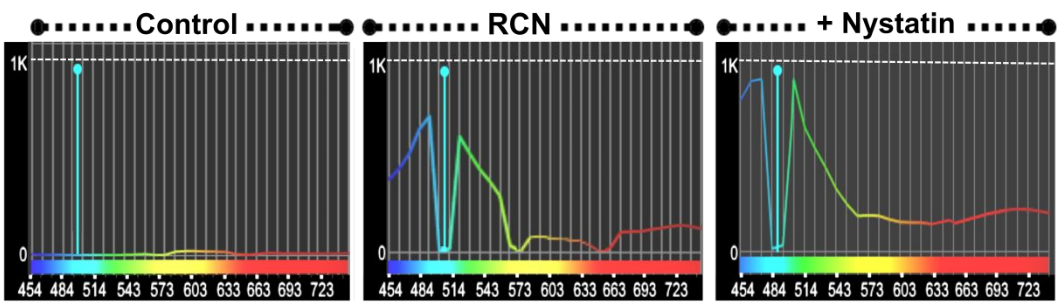

Figure 7. Spectrally-resolved confocal microscopy for real-time local fluorescence spectra of **RCN**. From left to right: non-stained SK-Lu-1 cells, 30 min incubation with 5 µM **RCN** and 50 µM nystatin treatment for 30 minutes. Cells were washed three-times before experiments. Excitation wavelength is 488 nm.

Then, spectral-resolution at the single-cell level revealed that nystatin-induced transmembrane pore formation leads to a strong enhancement of the green-channel emission band while a slight fluorescence increment in the red confocal channel thus providing a real-time local structural information of the *Naph* and *RCin* formation. Spectroscopic fluorescence titrations and imaging microscopy using nystatin and a series of transmembrane pore formation agents such as digitonin, etoposide and amphotericin A as well as oxidation, pH and lysis buffer controls is presented in the Supplementary Information file (Figures S7-S9), although similar effects were observed with other pore forming agents, nystatin produced stronger influences on both, fluorescence and subcellular localization profiles of the **RCN**, observing no probe interference with the pH or oxidation. Interestingly, the found polarity variation associated with osmotic pressure increments also indicate the mitochondrial membrane to be more hydrated after transmembrane pore formation by nystatin treatment, which is in agreement with recently described studies using optical super-resolution microscopic techniques.[31-33]

Finally, to correlate the morphological changes of the whole cell with the mitochondrial-bleb formation dynamics as a consequence of the transmembrane pore formation and osmotic pressure increments, the reorganization of the actin cytoskeleton upon nystatin dose was assessed. Cells expressing GFP-tagged actin were then imaged, Figure 8A. Actin framework distribution was successfully observed before the leakage of the cell content caused by lysis. After that, the *in-situ* addition of 5 μM **RCN** along with 100 μM nystatin (Figure 8B-C) allowed the observation of the actin microfilaments evidencing that those filaments were assembled on the bleb surroundings. While slight actin-cytosol equilibration is being initiated, the leakage of cell content is efficiently blocked by the cytoskeleton for the first few minutes (*ca.* 25 min). However, since the bleb formation continues and larger vesicle sizes are forming, the actin microfilaments and blebs start to lose their physical contacts, gaining thus a larger mobility as indicated by the bright green dots present in Figures 8C *vs.* 8B. Notably, for larger periods of time, the loss of actin organization during nystatin treatment also causes cell detachment which can lead to the spatial recording of different signals, thus interfering the analysis.

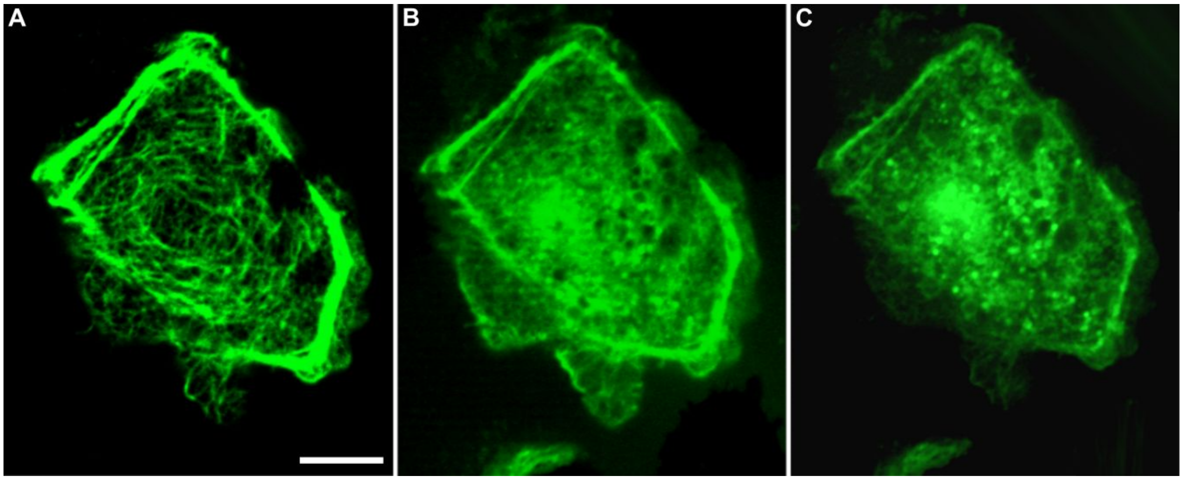

Figure 8. Confocal images of 5 µM **RCN** in SK-Lu-1 cells under 1 hour 100 µM nystatin treatment (A) prior transmembrane pore and bleb formation. (B) Small bleb vesicles formation after 25 min and (C) 45 min nystatin and **RCN** addition. Scale bar represents 10 µm.

CONCLUSION

The **RCN** probe provides a reliable protocol to assess the transmembrane pore formation driven osmotic pressure increments though polarity variations, a more robust physicochemical parameter allowing to measure the health and decease status of the cell. As strong morphology variations during bleb formation occur, the fluorescent probe described here was successfully utilized to analyze such complex subcellular scenario since the **RCN** provided a clear response to image the time-course distribution and associated mitochondrial-bleb dynamics, a challenging phenomenon whose monitoring could provide useful information of the physical implications of mitochondrial-bleb communication during cell death process. Using this new fluorophore architecture sensitive to membrane local polarity and super-resolution microscopy will provide a powerful tool for cell characterization using chemical, physical and physicochemical signaling.

ASSOCIATED CONTENT

Supporting Information.

The Supporting Information is available free of charge at http://pubs.acs.org spectroscopic ^{1}H and ^{13}C NMR data, HRMS data, UV-Vis and emission spectrophotometry, confocal microscopy figures, are provided in the supporting information file.

AUTHOR INFORMATION

Corresponding Author

arturo.jimenez@iquimica.unam.mx

ACKNOWLEDGMENT

Financial support by PAPIIT-UNAM IA200320 is greatefully acknowledge. We acknowledge the assistance of Evarardo Tapia Mendoza (MS), Ruth Rincón Heredia (PhD. Unidad de Imagenología, IFC-UNAM), Miguel Tapia Rodríguez (PhD. IIBO, UNAM) in imaging microscopy. Salvador Ramírez Jiménez (Biol. IIBO, UNAM) and Daniela Araiza-Olivera (PhD.) are aknowledge for assistance in tissue culture.

REFERENCES

1. Han, Y.; Li, M.; Qiu, F.; Zhang, M.; Zhang, Y.-H. Cell-Permeable Organic Fluorescent Probes for Live-Cell Long-Term Super-Resolution Imaging Reveal Lysosome-Mitochondrion Interactions. *Nat. Commun.* **2017**, *8, 1307*, doi:10.1038/s41467-017-01503-6

2. Schrader, M.; Godinho, L. F.; Costello, J. L.; Islinger, M. The Different Facets of Organelle Interplay–An Overview of Organelle Interactions. *Front. Cell Dev. Biol.* **2015**, *3*, 1–22.

3. Murley, A.; Nunnari, J. The Emerging Network of Mitochondria-Organelle Contacts. *Mol. Cell*, **2016**, *61*, 648–653.

4. Mayor, R.; Etienne-Manneville, S. The Front and Rear of Collective Cell Migration. *Nat. Rev. Mol. Cell Biol.* **2016**, *17*, 97–109.

5. Gauthier, N. C.; Fardin, M. A.; Roca-Cusachs, P.; Sheetz, M. P. Temporary Increase in Plasma Membrane Tension Coordinates the Activation of Exocytosis and Contraction During Cell Spreading. *Proc. Natl Acad. Sci. USA*, **2011**, *108*, 11467–11472.

6. Houk, A. R.; Jilkine, A.; Mejean, C. O.; Altschuler, S. J.; Wu, L. F.; Weiner, O. D. Membrane Tension Maintains Cell Polarity by Confining Signals to the Leading Edge During Neutrophil Migration. *Cell*, **2012**, *148*, 175–188.

7. Antonacci, G.; Braakman, S. Biomechanics of Subcellular Structures by Non-Invasive Brillouin Microscopy. *Sci. Rep.* **2016**, *6*, 37217.

8. Colom, A.; Derivery, E.; Soleimanpour, S.; Tomba, C.; Dal Molin, M.; Sakai, N.; González-Gaitán, M.; Matile, S.; Roux, A. A Fluorescent Membrane Tension Probe. *Nat. Chem.* **2018**, *10*, 1118–1125.

9. Goujon, A.; Colom, A.; Straková, K.; Mercier, V.; Mahecic, D.; Manley, S.; Sakai, N.; Roux, A.; Matile, S. Mechanosensitive Fluorescent Probes to Image Membrane Tension in Mitochondria, Endoplasmic Reticulum, and Lysosomes. *J. Am. Chem. Soc.* **2019**, *141*, 3380–3384.

10. Leiphart, R. J.; Chen, D.; Peredo, A. P.; Loneker, A. E.; Janmey, P. A. Mechanosensing at Cellular Interfaces. *Langmuir*, **2019**, *35*, 7509–7519.

11. Diz-Muñoz, A.; Weiner, O. D.; Fletcher, D. A. In Pursuit of the Mechanics that Shape Cell Surfaces. *Nat. Phys.* **2018**, *14*, 648−652.

12. Diz-Muñoz, A.; Thurley, K.; Chintamen, S.; Altschuler, S. J.; Wu, L. F.; Fletcher, D. A.; Weiner, O. D. Membrane Tension Acts Through PLD2 and Mtorc2 to Limit Actin Network Assembly During Neutrophil Migration. *PLoS Biol.* **2016**, *14*, e1002474.

13. Lieber, A. D.; Schweitzer, Y.; Kozlov, M. M.; Keren, K. Front-to-Rear Membrane Tension Gradient in Rapidly Moving Cells. *Biophys. J.* **2015**, *108*, 1599–1603.

14. Jiménez-Sánchez, A.; Lei, E. K.; Kelley, S. O. A Multifunctional Chemical Probe for Local Micropolarity and Microviscosity in Mitochondria. *Angew. Chem. Intl. Ed.* **2018**, *57*, 8891–8895.

15. Klymchenko, A. S.; Kreder, R. Fluorescent Probes for Lipid Rafts: From Model Membranes to Living Cells. *Chem. Biol. Rev.* **2014**, *21*, 97–113.

16. Jiang, N.; Fan, J.; Xu, F.; Peng, X.; Mu, H.; Wang, J.; Xiong, X. Ratiometric Fluorescence Imaging of Cellular Polarity: Decrease in Mitochondrial Polarity in Cancer Cells. *Angew. Chem. Intl. Ed. Engl.* **2015**, *54*, 2510–2514.

17. Kristanc, L.; Svetina, S.; Gomisček, G. Effects of the Pore-Forming Agent Nystatin on Giant Phospholipid Vesicles. *Biochim Biophys Acta*, **2012**, *1818*, 636–644.

18. Jokhadar, S. Z.; Božič, B.; Kristanc, L.; Gomisček, G. Osmotic Effects Induced by Pore-Forming Agent Nystatin: From Lipid Vesicles to the Cell. *PLoS ONE*, **2016**, *11,* e0165098. doi: 10.1371/journal.pone.0165098

19. Holz, R.; Finkelstein, A. The Water and Nonelectrolyte Permeability Induced in Thin Lipid Membranes by the Polyene Antibiotics Nystatin and Amphotericin B. *J. Gen. Physiol.* **1970**, *56*, 125–145.

20. Kleinberg, M. E.; Finkelstein, A. Single-Length and Double-Length Channels Formed by Nystatin in Lipid Bilayer Membranes. *J. Membr. Biol.* **1984**, *80*, 257–269.

21. Katsu, T.; Okada, S.; Imamura, T.; Komagoe, K.; Masuda, K.; Inoue, T.; Nakao, S. Precise Size Determination of Amphotericin B and Nystatin Channels Formed in Erythrocyte and Liposomal Membranes Based on Osmotic Protection Experiments. *Anal. Sci.* **2008**, *24*, 1551–1556.

22. Liu, X.; Hajnóczky, G. Altered Fusion Dynamics Underlie Unique Morphological Changes in Mitochondria During Hypoxia-Reoxygenation Stress. *Cell Death Differ.* **2011**, *18*, 1561–1572.

23. Long, Q.; Zhao, D.; Fan, W.; Yang, L.; Zhou, Y.; Qi, J.; Wang, X.; Liu, X. Modeling of Mitochondrial Donut Formation. *Biophys. J.* **2015**, *109*, 892–899.

24. Flores-Cruz, R.; López Arteaga, R.; Ramírez-Vidal, L.; López-Casillas, F.; Jiménez-Sánchez, A. Unravelling the Modus-Operandi of Chromenylium-Cyanine Fluorescent Probes: A Case Study. *Phys. Chem. Chem. Phys.* **2019**, *21*, 5779–15786.

25. Leung, C.W. T.; Hong, Y. N.; Chen, S. J.; Zhao, E. G.; Lam, J. W. Y.; Tang, B. Z. A Photostable AIE Luminogen for Specific Mitochondrial Imaging and Tracking. *J. Am. Chem. Soc.* **2013**, *135*, 62–65.

26. Yang, Z.; Cao, J.; He, Y.; Yang, J. H.; Kim, T.; Peng, X.; Kim, J. S. Macro-/Micro-Environment-Sensitive Chemosensing and Biological Imaging. *Chem. Soc. Rev.* **2014**, *43*, 4563–4601.

27. Charras, G. T.; Yarrow J. C.; Horton, M. A.; Mahadevan, L.; Mitchison, T. J. Non-Equilibration of Hydrostatic Pressure in Blebbing Cells. *Nature*, **2005**, *435*, 365–369.

28. Charras, G. T.; Coughlin, M.; Mitchison, T. J.; Mahadevan, L. Life and Times of a Cellular Bleb. *Biophys J.* **2008**, *94*, 1836–1853.

29. Vaux, D. L.; Wilhelm, S.; Häcker, G. Requirements for Proteolysis During Apoptosis. *Mol. Cell Biol.* **1997**, *17*, 6502–6507.

30. Chang, H. Y.; Yang, X. Proteases for Cell Suicide: Functions and Regulation of Caspases. *Microbiol. Mol. Biol. Rev.* **2000**, *64*, 821–846.

31. Moon, S.; Yan, R.; Kenny, S. J.; Shyu, Y.; Xiang, L.; Li, W.; Xu, K. Spectrally Resolved, Functional Super-Resolution Microscopy Reveals Nanoscale Compositional Heterogeneity in Live-Cell Membranes. *J. Am. Chem. Soc.* **2017**, *139*, 10944–10947.

32. Yan. R.; Moon, S.; Kenny, S. J.; Xu, K. Spectrally Resolved and Functional Super-resolution Microscopy via Ultrahigh-Throughput Single-Molecule Spectroscopy. *Acc. Chem. Res.* **2018**, *51*, 697–705.

33. Danylchuk, D. I.; Moon, S.; Xu, K.; Klymchenko, A. K. Switchable Solvatochromic Probesfor Live-Cell Super-resolution Imaging of Plasma Membrane Organization. *Angew. Chim. Int. Ed. Engl.* **2019**, *58*, 14920–14924.

ToC Graphic